Environ. Sci. Technol. **2011,** *45,* 984–991

Formation of Nitrogen-Containing Oligomers by Methylglyoxal and Amines in Simulated Evaporating Cloud Droplets

DAVID O. DE HAAN,*,†,‡
LELIA N. HAWKINS,†
JULIA A. KONONENKO,†
JACOB J. TURLEY,†
ASHLEY L. CORRIGAN,†,§
MARGARET A. TOLBERT,‡ AND
JOSE L. JIMENEZ‡

Department of Chemistry and Biochemistry, University of San Diego, San Diego, California 92110, United States and Cooperative Institute for Research in Environmental Sciences and Department of Chemistry and Biochemistry, University of Colorado at Boulder, Boulder, Colorado 80309, United States

Received August 25, 2010. Revised manuscript received November 17, 2010. Accepted November 18, 2010.

Reactions of methylglyoxal with amino acids, methylamine, and ammonium sulfate can take place in aqueous aerosol and evaporating cloud droplets. These processes are simulated by drying droplets and bulk solutions of these compounds (at low millimolar and 1 M concentrations, respectively) and analyzing the residuals by scanning mobility particle sizing, nuclear magnetic resonance, aerosol mass spectrometry (AMS), and electrospray ionization MS. The results are consistent with imine (but not diimine) formation on a time scale of seconds, followed by the formation of nitrogen-containing oligomers, methylimidazole, and dimethylimidazole products on a time scale of minutes to hours. Measured elemental ratios are consistent with imidazoles and oligomers being major reaction products, while effective aerosol densities suggest extensive reactions take place within minutes. These reactions may be a source of the light-absorbing, nitrogen-containing oligomers observed in urban and biomass-burning aerosol particles.

Introduction

Between 80% and 95% of submicrometer particles in the troposphere contain significant amounts of organic material (*1, 2*), which can affect climate (*3*) through changes in aerosol optical properties (*4*) and hygroscopicity (*5, 6*). The majority of this organic material is usually secondary in nature, especially for submicrometer particles (*7*) and for cloud-processed particles near 1 μm diameter (*1*). Recent studies have found that many organic aerosol particles sampled in urban air (*8*) or generated from biomass burning (*9*) contain nitrogen-containing oligomerized material, but the reactions responsible for the particle-phase formation of these oligomers are not known.

Model estimates attribute as much as one-third of global SOA production to aerosol formation by α-dicarbonyl compounds, especially methylglyoxal (*10*) and glyoxal (*11*), if the uptake of these compounds by clouds and aerosol is irreversible. Direct measurements of glyoxal in Mexico City coupled with kinetic model predictions indicate that glyoxal accounts for at least 15% of total SOA formation there (*12*); a SOA sink for gas-phase glyoxal also improves discrepancies between measured and predicted glyoxal concentrations. Glyoxal can react with itself to form oligomers as it is taken up by aerosol (*13*), but irreversible reactions such as photooxidation (*14, 15*) and reaction with ammonium salts (*16*−*18*) and amines (*19, 20*) are more important in aerosol formation in aqueous particles (*21*). These latter reactions form imidazoles (*16, 19, 20*) and light-absorbing compounds (*17, 18*), likely through iminium ion intermediates (*18*).

Less is known about the atmospheric chemistry of methylglyoxal. The atmospheric production and aqueous-phase processing of glyoxal and methylglyoxal are summarized in Scheme 1. Both glyoxal and methylglyoxal are formed mainly by isoprene oxidation (*10, 11*). Some (*22, 23*) but not all (*24*) studies indicate that methylglyoxal is scavenged by aqueous aerosol from the gas phase. Both compounds are oxidized at the same rate by aqueous OH radicals (*25*), forming organic acids and oligomers (*15, 26*). While both can also self-oligomerize upon droplet evaporation, the mechanisms are different: glyoxal forms acetal oligomers (*13*), while methylglyoxal reacts mainly by aldol condensation (*27*). A recent study of methylglyoxal reactivity in ammonium salt solutions demonstrated the formation of light-absorbing oligomer compounds by aldol condensation reactions (*28*). At pH ≥ 7.8 and 37 °C, methylglyoxal is known to form radical intermediates and fluorescent, light-absorbing melanoidin products upon reaction with amino acids (*29*). In this work, we study the aqueous, room-temperature reactions of methylglyoxal with ammonium sulfate, methylamine, and several amino acids present in clouds. In the first two parts, we present nuclear magnetic resonance (NMR), aerosol mass spectrometry (AMS), and electrospray ionization (ESI)-MS data and identify a variety of methylimidazole and nitrogen-containing oligomer products in bulk-phase reactions. In the third part, we describe AMS studies of aerosol formed by drying aqueous droplets and show that these reaction products are detected on a time scale of minutes. In the last part, we discuss effective aerosol density measurements which indicate complete reaction within several minutes after drying.

Methods

Reaction solutions were generated in deionized water or D_2O (Cambridge Isotope, 99.9% D) from 40% w/w methylglyoxal solution (Alfa-Aesar), 97% glyoxal trimer dehydrate, 40% w/w methylamine solution, 99% glycine, serine, ornithine HCl, ammonium sulfate, 98% aspartic acid, and arginine (all Sigma-Aldrich), used without further purification. Experimental methods have been described earlier (*19, 20*) and are briefly outlined here. Bulk aqueous samples (0.5−1.0 M) were dried in 150 μL aliquots under ambient conditions. Resulting brown solids were redissolved for structural determination in deionized water at 1 mg/mL for ESI-MS or time-of-flight high-resolution (HR-ToF-) AMS analysis (*30*) or in D_2O for NMR analysis. Cloud droplet drying was simulated by generating ∼5 μm wet diameter droplets from 4 to 8 mM solutions using an ultrasonic nebulizer (*19*), neutralizing their static charge, and sampling them from a 300 L collapsible

* Corresponding author phone: (619) 260-6882; fax: (619) 260-2211; e-mail: ddehaan@sandiego.edu.
† University of San Diego.
‡ University of Colorado.
§ Currently at Scripps Institution of Oceanography, University of California, San Diego, California 92037.

10.1021/es102933x

Published on Web 12/20/2010

SCHEME 1. Products Formed during Aqueous-Phase Processing of Glyoxal and Methylglyoxal[a]

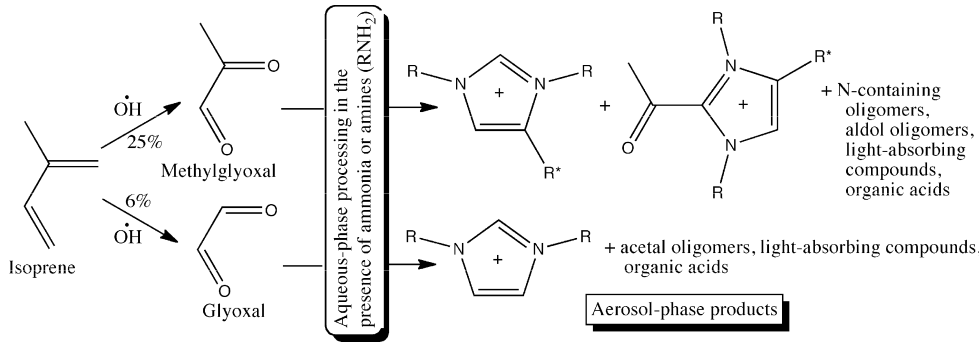

[a] Globally averaged multistep isoprene oxidation yields from ref (*10*).

Teflon chamber containing humidified N_2 by size-calibrated scanning mobility particle sizing (SMPS), quadrupole (Q-) AMS (*31*), and/or HR-ToF-AMS instruments operating at a 600 °C aerosol vaporization temperature and 70 eV electron impact ionization. Sampling lines were copper or conductive polymer tubing. Relative humidity (RH) was recorded at the chamber outlet by a Vaisala sensor (HMT337) and was kept between 60% and 90% RH.

Effective densities were calculated for some aerosol populations by fitting SMPS and Q-AMS size distributions to log-normal distributions. The geometric mean diameters measured by the two methods are related by the effective density (*32*)

$$D_{SMPS} = \rho_{eff} D_{AMS} \quad (1)$$

Results and Discussion

Imidazole Product Identification. In the reactions of glyoxal with ammonium sulfate (*16*) and amines (*19, 20*), the two major products observed were imidazoles and diimines, with larger oligomers detected only for the reaction with methylamine and side-chain reaction products detected only for arginine. ESI mass spectra of the products of bulk-drying reactions between methylglyoxal and amino acids, ammonium sulfate, and methylamine are shown in Figure 1. No diimines are detected, but in all cases, methyl analogs of other glyoxal products are observed (*16, 19, 20*). For example, arginine forms 1:1 adducts with methylglyoxal (*m/z* 247, 229) by reaction at the arginine side chain, followed by water loss. The *m/z* 247 adduct structure, elucidated using NMR data (Table S1, Supporting Information), differs from the major product of the glyoxal + arginine reaction (*19*) by addition of a single methyl group. Dominant peaks consistent with the formation of *N*-derivatized 4-methyl imidazoles ("methylimidazole" in Scheme 2) are detected for reactions of methylglyoxal with the other amine compounds: glycine (*m/z* 199), serine (*m/z* 259), aspartic acid (*m/z* 315), ornithine (*m/z* 313), and methylamine (*m/z* 111), while ammonium sulfate forms underivatized methylimidazole (*m/z* 83). A minor peak (*m/z* 397) in the mass spectrum of the arginine reaction products may also be the methylimidazole product (*16, 19, 20*). As with glyoxal, the carbon atom between the two nitrogen atoms in the imidazole ring appears to come from a second dicarbonyl molecule (as shown in Scheme 2), for reasons described below.

Other major peaks are consistent with unique products (black boxes in Scheme 2) that have no analogs in corresponding glyoxal reactions. Imine dimers, where both methylglyoxal molecules are still intact and incorporated into an imidazole ring, are consistent with major peaks detected by ESI-MS (labeled blue in Figure 1) for reactions with glycine (*m/z* 241), serine (*m/z* 301), ammonium sulfate (*m/z* 125),

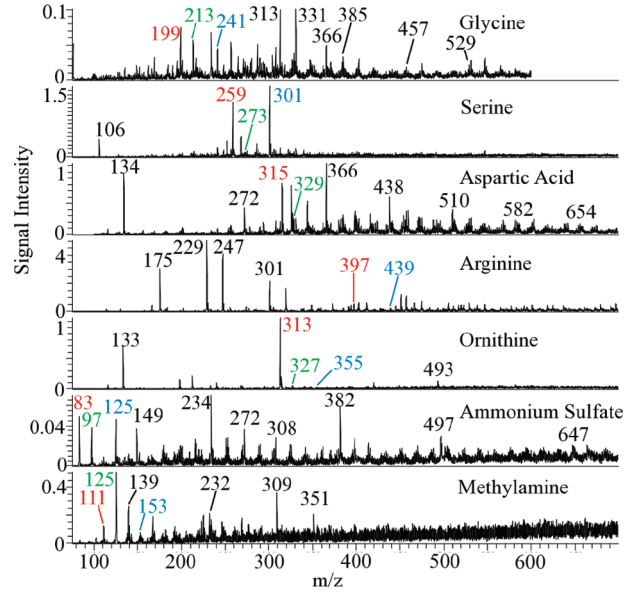

FIGURE 1. ESI-mass spectra of products of the reactions of methylglyoxal with amino acids, ammonium sulfate, and methylamine. Peak *m/z* values labeled red, methylimidazole products (analogous to imidazoles formed by glyoxal); green, dimethylimidazole products; blue, imine dimers. A signal height of 1 in each graph is equivalent to 10^6 MS ion counts. For experiments with glycine, serine, or aspartic acid, solutions contained 0.05 M of each reactant before drying under ambient conditions. For experiments with ornithine or arginine, solutions contained 0.5 M of methylglyoxal, acetic acid to reduce the pH to 5, and either 0.5 M ornithine or 0.4 M arginine before drying. All solutions were reconstituted in water at 1 mg/mL (assuming no solute evaporated).

and methylamine (*m/z* 153) and with minor peaks detected for reactions with arginine (*m/z* 439) and ornithine (*m/z* 355). The presence of these dimers supports the idea that all carbons in the methylimidazole ring can come from dicarbonyls, as proposed previously (*19*). A 2,4-dimethylimidazole product is consistent with major peaks observed by ESI-MS (labeled green, Figure 1) in reactions with glycine (*m/z* 213), ammonium sulfate (*m/z* 97), and methylamine (*m/z* 125) and with minor peaks observed in reactions with serine (*m/z* 273), aspartic acid (*m/z* 329), and ornithine (*m/z* 327). A methyl group in the 2 position on an imidazole ring can be assumed to come from incorporation of acetaldehyde. This is puzzling because acetaldehyde was not added in this study as a reactant nor is it the C_2 fragment one would expect from methylimidazole formation (*19, 29*).

SCHEME 2. Potential Structures of Imidazoles and Oligomers Formed in Reactions of Methylglyoxal with Amines and Ammonium Salts[a]

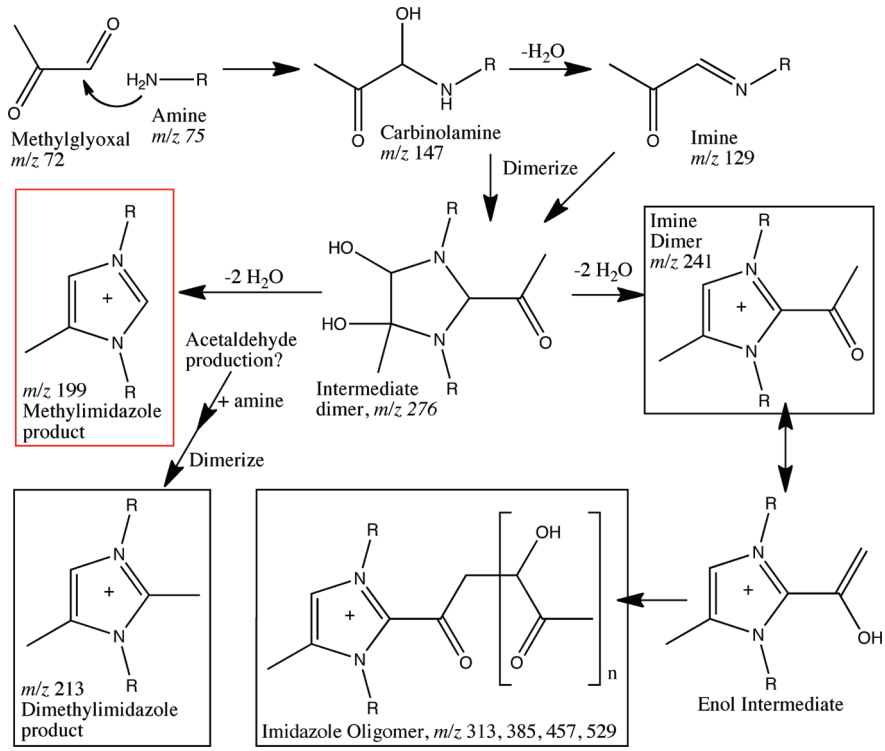

[a] All *m/z* ratios are given for glycine, R = CH_2COOH. Boxes designate structures consistent with NMR signals and with masses detected by positive-mode ESI-MS (Figure 1), with neutral molecules shown here detected as protonated $M+1$ ions. Red box designates the methyl analog of the product observed in glyoxal reactions.

Assignment of major ESI-MS peaks to imidazole derivatives is consistent with ^{1}H and ^{13}C NMR data collected on identical methylglyoxal/amine reaction mixtures that were dried and redissolved in D_2O instead of water. Peak assignments are listed in Tables S1−S3, Supporting Information. Characteristic peaks for methylimidazoles are an equal-sized pair of singlets at ~7.1 and ~8.7 ppm (visible for every amine studied), while imine dimers (glycine, serine, and ornithine reactions) and dimethylimidazoles (glycine and ornithine reactions) have singlet peaks at ~8.1 and ~6.8, respectively. These latter two products were not observed by NMR for reactions of methylglyoxal with aspartic acid.

The chemical formulas of the proposed imidazole products were confirmed by accurate mass measurements by HR-ToF-AMS on bulk-dried samples. For the reaction of methylglyoxal with glycine, the accurate mass of the *m/z* 199, 213, and 241 peaks was consistent with *N*-derivatized methylimidazole ($C_8H_{11}N_2O_4$, m/z = 199.07), dimethylimidazole ($C_9H_{13}N_2O_4$, m/z = 213.08), and imine dimer ($C_{10}H_{13}N_2O_5$, m/z = 241.08) products, respectively. ESI-MS analysis of the products of the reaction of methylglyoxal with ^{15}N-labeled glycine confirmed that molecules containing two labeled nitrogen atoms were responsible for all three peaks. Finally, elemental H/C, O/C, and N/C ratios measured by HR-ToF-AMS (*33*), shown as filled circles in Figure 2 (and Figures S1 and S2 and Tables S4−S6, Supporting Information) were consistent, within uncertainties, with the range of theoretical ratios for the proposed imine and imidazole products (open symbols) for every *bulk-phase* methylglyoxal reaction tested (glycine, serine, ornithine, and methylamine). This suggests that imine and imidazole products are major components produced in bulk-phase reactions of methylglyoxal with amines and ammonium sulfate.

Oligomer Characterization. A significant, unique feature of the ESI-mass spectra (Figure 1) is clear evidence of oligomer formation found for all methylglyoxal reactions. With the exception of methylamine (*20*), no oligomers were observed for corresponding glyoxal reactions studied under identical bulk-drying conditions (*19*). With methylglyoxal, signals elevated to at least 10 times background are observed extending to at least m/z 700, with prominent peaks separated by repeated distances of $\Delta m/z = 2$ and in most cases $\Delta m/z = 18$. Patterns of $\Delta m/z = 2$ are consistent with incorporation of variable numbers of nitrogen and oxygen atoms into oligomer structures (*34, 35*). Furthermore, a wave pattern with $\Delta m/z = 18$ is clearly seen for methylglyoxal reactions with glycine, aspartic acid, and ammonium sulfate and is present but less pronounced with serine, arginine, and ornithine reactions. This $\Delta m/z = 18$ pattern suggests repeated additions or losses of water (m/z 18) and methylglyoxal oligomer units (m/z 72). The strong $\Delta m/z = 72$ patterns observed with aspartic acid (m/z 366, 438, 510, 654) and glycine (m/z 313, 385, 457, 529) support this assignment.

Although $\Delta m/z = 18$ patterns were also observed by ESI-MS with methylglyoxal in the absence of amines (*27*), two lines of evidence suggest that in the presence of amines most oligomer molecules incorporate nitrogen. First, the locations of $\Delta m/z = 18$ oligomer peak series vary with the amine, which would not be the case without amine incorporation. For example, the $\Delta m/z = 18$ pattern observed by ESI-MS for methylglyoxal reactions with ammonium sulfate and glycine are out of phase from each other by ~7 amu, and the methylglyoxal/arginine system displays a unique $\Delta m/z = 6$ pattern likely due to three overlapping $\Delta m/z = 18$ patterns. Second, the observed N/C ratios in the bulk products (filled circles in Figure 2) would be much lower if many of the

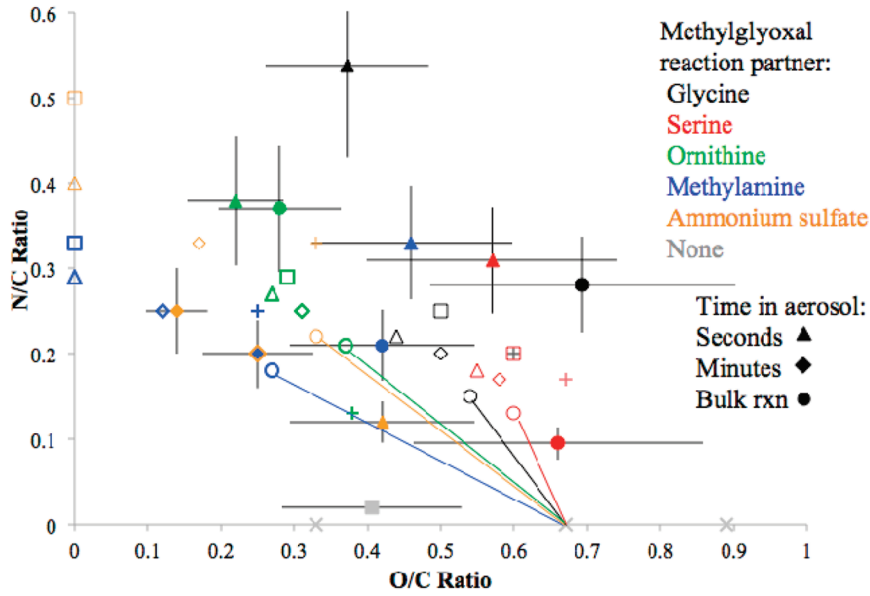

FIGURE 2. N/C and O/C elemental ratios provided by HR-ToF-AMS (filled symbols) and predicted (open symbols) for reaction products of methylglyoxal with glycine (black), serine (red), ornithine (green), methylamine (blue), ammonium sulfate (orange), and methylglyoxal self-reactions (gray). Error bars are $\pm 1\sigma$. Bulk-phase reactions: filled circles, all concentration 1 M except for 0.5 M serine. Aerosol phase reactions are shown according to time from droplet generation to aerosol sampling: 10−40 min (filled diamonds) or ~5 s (filled triangles), all concentrations 4−8 mM. Predicted ratios: imine oligomers (open circles with diagonal lines indicating range of values), imine dimers (open diamonds), methylimidazoles (open squares), dimethylimidazoles (open triangles), imines (+), and methylglyoxal self-reactions (×). All values are listed in Tables S4 and S5, Supporting Information.

oligomer peaks seen in Figure 1 were due to methylglyoxal oligomers that did not incorporate nitrogen. We conclude that methylglyoxal is not simply reacting with itself to form oligomers and with amines to form imidazole monomers in our experiments; rather, both processes are acting on the same molecules to form complex, nitrogen-containing oligomers.

The $\Delta m/z = 2$ pattern suggests that many different oligomer structures are formed by the reaction of methylglyoxal with amines, as mentioned above. However, we note that the $\Delta m/z = 72$ series of peaks (and associated $\Delta m/z = 18$ series) that are most strongly detected by ESI-MS emanate from a base peak assigned to the imine dimer for methyglyoxal reactions with glycine, serine, ornithine, ammonium sulfate, and methylamine. Furthermore, the dimer-based $\Delta m/z = 72$ series is not observed for reactions where the imine dimer was weak (arginine) or not observed (aspartic acid). (With aspartic acid, the strongest $\Delta m/z = 72$ series emanates from an unassigned peak at m/z 366.) This suggests that the imine dimer can initiate aldol condensation reactions with its enol-forming acetyl moiety, forming oligomers by reacting with methylglyoxal as shown in Scheme 2 and presumably also reacting with imines.

The structures of the oligomers formed in methylglyoxal/aspartic acid reactions were also probed in an ESI-MS-MS ion map experiment, where every product peak from m/z 70 to 700 was fragmented sequentially in the ion trap. Figure S3, Supporting Information, summarizes the fragments observed, and Figure S4 shows the mass spectrum overlaid with neutral loss spectra for parent ions between m/z 300 and 400. Most peaks beyond m/z 300 fragmented by loss of units of water ($\Delta m/z$ 18 and 36), methylglyoxal ($\Delta m/z$ 72, 144), aspartic acid ($\Delta m/z$ 133), and combinations of these (e.g., methylglyoxal and water, $\Delta m/z$ 90). For example, peaks at m/z 333 and 334 notably fragmented via loss of aspartic acid ($\Delta m/z$ 133) with fragment ion abundances of $>2 \times 10^5$. However, there were 28 other ions between m/z 300 and 400 that lost an aspartic acid group with fragment ion abundances at least twice typical baseline levels (3×10^3). These common fragmentation patterns seen in oligomer peaks across the mass spectrum appear as diagonal stripes in Figure S3, Supporting Information. These observations demonstrate that methylglyoxal/aspartic acid building blocks form a large array of nitrogen-containing oligomer structures, likely by aldol condensation of methylglyoxal and methylglyloxal/aspartic acid imine units onto various core molecules.

The reaction products of methylglyoxal/methylamine exhibit in ESI-MS a unique $\Delta m/z = 13$ oligomer peak spacing at lower m/z and a featureless, elevated signal at higher masses (Figure 1) which is more than 100 times above background. The $\Delta m/z = 13$ pattern can be attributed to methylamine addition ($+m/z$ 31) followed by water loss ($-m/z$ 18), as seen in reactions with glyoxal (*20*). When combined with additions of methylglyoxal (m/z 72), imine (m/z 71) (neither divisible by 13), and the multiplicity of oligomer structures ($\Delta m/z$ 2 peaks), the patterns interfere with each other, resulting in featureless, elevated signals beyond $m/z \approx 300$. Similar effects can be observed with amino acids but only at much higher m/z values because of amino acids' larger molecular masses.

Aerosol-Phase Product Detection. We reported thus far on the products of methylglyoxal reactions formed in bulk-phase drying experiments where reactant concentrations are 4−6 orders of magnitude above cloud concentrations (*36*−*41*), and drying times are on the order of days. Computational work on methylglyoxal self-reactions (*42*) suggests that reaction pathways (acetal formation vs aldol condensation) may depend on experimental conditions (i.e., on whether a system is under kinetic or thermodynamic control). In order to determine whether the reaction products described above also form at atmospherically relevant short reaction times and lower concentrations, we performed experiments where aqueous droplets were generated containing the reactants at low millimolar concentrations and sampled over time scales of seconds to minutes. Elemental ratios measured by HR-ToF-AMS during these experiments are shown in Figure 2 (and Figures S1 and S2 and Tables S4−S6, Supporting Information).

In the first set of experiments, droplets containing methylglyoxal and ammonium sulfate (sometimes in combination with methylamine) were held in a humid chamber at ~80% RH and the resulting aerosol was sampled for 15 min by AMS. Whether or not methylamine was present, the N/C and O/C elemental ratios of the organic aerosol fraction were within the expected range of imidazole products (Figure 2), although the H/C ratio was somewhat higher (Figures S1 and S2, Supporting Information). Many product peaks were detected by HR-ToF-AMS. Although unreacted ammonium sulfate signals dominated the mass spectra in both cases, for methylglyoxal + ammonium sulfate large peaks matched the accurate mass for the product ions CH_3NH (m/z 30.034), CH_3NH_2 (m/z 31.042), CH_3N (m/z 29.026), and CHN (m/z 27.011), while small peaks matched up with the ions C_2H_4N (m/z 42.034) and C_3H_4N (m/z 54.034, peaks listed in descending order of size). All of these detected ions are consistent with the formation of imine products in less than 15 min. When methylamine was also present (in a 40 min experiment), the peaks from m/z 27 to 31 can no longer be assigned only to products but the m/z 42 and 54 peaks listed above are still detectable, along with other imine fragments C_3H_6N (m/z 56.05), C_3H_7NO (m/z 73.05), and likely imidazole species $C_4H_6N_2$ (m/z 82.05), $C_5H_7N_2$ (m/z 95.06), and $C_7H_{13}N_2$ (m/z 125.11).

A similar experiment was performed on droplets containing 5 mM methylglyoxal and glycine held in a chamber held between 77% and 87% RH. Over a 25 min sampling period, peaks were detected by Q-AMS at m/z 111 and 125. These peaks were also observed in HR-ToF-AMS analyses of bulk-dried products for the same reaction system at m/z 111.09 and 125.11, which match the imidazole fragments $C_6H_{11}N_2$ and $C_7H_{13}N_2$, respectively.

The m/z 125 peak was notably absent in a "short" experiment where droplets containing 4 mM each methylglyoxal and glycine bypassed the chamber and were sent directly into the AMS via a diffusion dryer, indicating that imidazole formation requires reaction times greater than a few seconds. (The lower RH of the diffusion dryer compared to chamber experiments should, by itself, favor reactions.) In a similar set of short experiments, droplets containing methylglyoxal and either serine, ornithine, or methylamine were also sent directly to the AMS via a diffusion dryer. Resulting elemental ratios are shown as filled triangles in Figure 2 (and Figures S1 and S2, Supporting Information). With the exception of ornithine, measured ratios are significantly different than those measured for bulk-phase reaction products and for the chamber drying experiments just described. The measured elemental ratios of glycine aerosol and methylglyoxal aerosol formed under similar short conditions (from 7.5 and 4.0 mM solutions, respectively) are listed in Tables S4−S6, Supporting Information, for comparison. For the short methylglyoxal/glycine experiment, the elemental ratios are roughly midway between the measured ratios of the two reactants, consistent with minimal reaction taking place in only a few seconds.

Furthermore, ions detected by HR-ToF-AMS in these experiments also suggest that little imidazole formation has occurred after only ~5 s of reaction time. For runs where methylglyoxal was mixed with either glycine or serine, HR-ToF-AMS peaks are almost entirely attributable to unreacted amino acid, methylglyoxal, and methylglyoxal oligomers, with only a few minor exceptions such as C_4H_6NO (m/z 84.05) and $C_4H_6NO_2$ (m/z 100.04), both likely imine fragments. For the reaction with ornithine, small peaks are detected that match $C_7H_9N_2$ (m/z 121.08) and $C_8H_{11}N_2$ (m/z 135.09). These peaks, which were also detected in bulk-phase reactions for this system, appear to be imine rather than imidazole fragments due to their high H/C ratios. For methylglyoxal and methylamine, uniquely, the AMS spectrum is dominated by product peaks after only 5 s. In descending order of peak height, detected peaks match the ions NO (m/z 30.00), NO_2 (m/z 45.99), C_2H_4N (m/z 42.03), C_3H_6N (m/z 56.05), C_5H_8N (m/z 82.07), C_6H_8NO (m/z 110.06), and C_7H_8NO (m/z 122.06). None of these peaks, however, are likely from imidazole products, and the imidazole peaks observed in the corresponding bulk reaction are not detected at ~5 s. Methylglyoxal/methylamine mixtures were the only ones to turn yellow immediately upon mixing at these concentrations, indicating that at least some of the products observed at short reaction times likely formed in bulk solution before droplet generation. These mixtures were also the only ones with pH > 7, and preliminary studies in our lab suggest that methylglyoxal/amine reactions are faster at high pH.

To summarize, there is evidence for detectable imidazole product formation in less than 30 min in residual aerosol containing methylglyoxal and either glycine or methylamine. Imidazole formation appears to have taken place in the aerosol phase in minutes after the drying process, rather than in the bulk phase before aerosol generation, since imidazole products are not detectable in any aerosol that was sampled only ~5 s after droplet generation. Our data suggests that imines, which are intermediates in imidazole formation, can form to a limited extent either immediately upon solution mixing or within seconds of droplet generation. The nitrogen-containing oligomers detected by ESI-MS cannot be distinguished from methylimidazole products by AMS due to heavy fragmentation by electron ionization. However, they would not be expected to form any faster than the methylimidazole products.

Aerosol Densities. Aerosol densities were measured using SMPS and Q-AMS particle time-of-flight traces with signals above 3× noise (*43*) by fitting each to log-normal distributions and using the effective density to match geometric mean diameters (*44*). For runs with ammonium sulfate, aerosol was diffusion dried before equilibrating in the chamber. For other runs, aerosol was sent directly to the humid chamber for equilibration. Glycine effloresces at 55% RH (*45*), while ammonium sulfate does so at 35% RH (*46*). Experimental RH in runs involving these substances did not fall below these values, so particles should be in a liquid state rather than a solid state even if little reaction occurred. For the run with methylglyoxal and methylamine, the mixture of products would not be expected to crystallize at any RH. Thus, all resulting aerosol can be assumed spherical under ambient conditions. However, particles lose water upon entering the AMS inlet and could crystallize then, becoming nonspherical (*47*). If particles remain spherical, the effective densities measured by this method (Table 1) will equal actual material densities; otherwise, measured densities will be lower (*32*).

In no case were measured effective densities time dependent, indicating that particles have equilibrated with water vapor and that reactions are essentially complete within several minutes that elapse between droplet generation and first analysis. This suggests that either nitrogen-containing oligomers form at similar time scales as methylimidazole products or the two products have similar densities in every case. Our effective density data, described below, suggests that the two products have different densities, leading us to conclude that they likely form at similar time scales, thereby allowing measured effective densities to be constant.

The particles must consist of some mixture of reaction products, low-volatility reactants such as glycine or ammonium sulfate, and/or water. The volatile compounds methylglyoxal, methylamine, and glyoxal should all evaporate from drying droplets unless they take part in a reaction, and much of the water may evaporate in the AMS inlet. The effective density of methylglyoxal/glycine aerosol (1.74 ± 0.04

TABLE 1. Effective Aerosol Densities Measured for Aerosol Dried from Aqueous Droplets

initial conc. (mM)	reactants present in droplets	chamber	RH (%)	sampling time (min)	effective density (g/cm^3)
5 and 10	methylglyoxal, methylamine	yes	72−84	60	1.62 ± 0.04
5	methylglyoxal, glycine	yes	77−87	100	1.74 ± 0.07
5	glyoxal, glycine	yes	60−80	15	2.00 ± 0.04
2	methylamine, ammonium sulfate	yes	77[a]	20	1.43 ± 0.02
2	glyoxal, methylamine, ammonium sulfate	yes	84[a]	20	1.48 ± 0.02
16	methylglyoxal	yes	58[a]		1.9 ± 0.1[b]
0.14	glyoxal	no	*c*		1.71 ± 0.02[b,d]
4	glycine	no	*c*		1.18 ± 0.06[b]
	ammonium sulfate (dry)				1.74[e]

[a] Aerosol passed through a diffusion dryer en route to the humid chamber. [b] Reference (*27*). [c] Aerosol passed through a diffusion dryer en route to AMS and SMPS. [d] Matches bulk density (*16*). [e] Calculated value for comparison, based on a shape factor of 1.02 (*46*) and bulk density of dry ammonium sulfate of 1.77 g/cm^3.

g/cm^3) is between that of aerosol containing either methylglyoxal (1.9 ± 0.1 g/cm^3) or glycine (1.18 ± 0.06 g/cm^3) alone but closer to that of methylglyoxal. This suggests that a significant quantity of methylglyoxal remains in the aerosol via either self-reactions or reactions with glycine. The high and constant density suggests that minimal water is present, even as RH levels rose from 77% to 87% during 100 min of measurements.

Interestingly, for aerosol containing glyoxal and glycine, the effective density (2.00 ± 0.04 g/cm^3) is higher than that for aerosol containing either glyoxal (1.71 ± 0.02 g/cm^3) or glycine (1.18 ± 0.06 g/cm^3) alone. Since this reaction produces *N*-derivatized imidazole salts but not oligomers (*19*), this indicates that the imidazole salts have a density ≥ 2.0 g/cm^3, which is significantly higher than the effective aerosol density measured for aerosol produced by any methylglyoxal/amine reaction, where nitrogen-containing oligomers would be expected to be present along with methylimidazole salts.

The lower effective density of methylglyoxal/methylamine aerosol (1.62 ± 0.04 g/cm^3) compared to methylglyoxal aerosol (1.9 ± 0.1 g/cm^3) suggests that methylglyoxal has reacted more with methylamine than with itself, consistent with expectations based on nucleophilic strength and with experiments on glyoxal (*20*). The bulk densities of liquid methylamine and methylamine solutions are <1 g/cm^3, but aerosol particles containing only methylamine and water evaporate so extensively that the resulting particles are too small to measure effective aerosol density by this method. It is unlikely that the lower effective density of methylglyoxal/methylamine aerosol is due to high water content, since analogous glyoxal/methylamine aerosol do not shrink in size as RH drops from 80% to 50% (Figure S5, Supporting Information).

The density of ammonium sulfate/methylamine aerosol (1.43 ± 0.02 g/cm^3) is expected to be due to a combination of ammonium and methylammonium sulfate salts and water, since methylamine can be protonated by ammonium ions. In addition, the measured effective density is between those of solid ammonium sulfate aerosol (ρ_{eff} = 1.74 g/cm^3) (*46*) and saturated ammonium sulfate solutions (ρ_{eff} = 1.24 g/cm^3) (*48*). The addition of glyoxal to this system slightly increases the overall effective density to 1.48 ± 0.02 g/cm^3, most likely due to oligomer products of reactions of glyoxal with methylamine (*20*) or ammonium sulfate (*16*−*18*).

In summary, measured effective densities for aerosol generated from methylglyoxal and either methylamine or glycine at low millimolar concentrations suggest that reactions have occurred to significant extents within several minutes of drying, in agreement with AMS measurements. Although atmospheric temperatures are lower and initial cloudwater concentrations are 2−4 orders of magnitude below those used in this study, we note that atmospheric aerosol particle lifetimes are on the order of days, significantly longer than our aerosol experiments. The speed of product formation observed in aerosol formed from drying water droplets in this work suggests that these reactions will occur in drying cloud droplets in the atmosphere, forming nitrogen-containing oligomers, light-absorbing melanoidins, and methylimidazole salts that will remain in the aerosol phase. If these reactions occur at high rates in atmospheric aqueous aerosol, they may explain why oligomers observed in urban aerosol contain nitrogen (*8*) and correlate with amine signals (*49*).

Methylated imidazoles were recently found to be the dominant nitrogen-containing organic species in lab-generated biomass burning aerosol (*9*). While the production of these substances has been ascribed to the pyrolysis of biopolymers (*50*), we note that methylglyoxal is formed as sugars break down at high temperatures (*51*). This work suggests that the room-temperature, aqueous-phase reactions of methylglyoxal with amine compounds may create similar brown-carbon material as biomass burning but at a much slower rate.

Acknowledgments

This work was supported by NSF grant ATM-0749145. D.D.H. was supported by a CIRES Fellowship.

Supporting Information Available

NMR peak assignments, HR-ToF-AMS elemental ratios and graphs, ESI-MS fragmentation data for methylglyoal/aspartic acid oligomers, and SMPS size distribution data for glyoxal/methylamine aerosol being dried from 81% to 50% RH. This material is available free of charge via the Internet at http://pubs.acs.org.

Literature Cited

(1) Bahadur, R.; Russell, L. M.; Prather, K. Composition and morphology of individual combustion, biomass burning, and secondary organic particle types obtained using urban and coastal ATOFMS and STXM-NEXAFS measurements. *Aerosol Sci. Technol.* **2010**, *44* (7), 551–562.

(2) Murphy, D. M.; Cziczo, D. J.; Froyd, K. D.; Hudson, P. K.; Matthew, B. M.; Middlebrook, A. M.; Peltier, R. E.; Sullivan, A.; Thomson, D. S.; Weber, R. J. Single-particle mass spectrometry of tropospheric aerosol particles. *J. Geophys. Res.* **2006**, *111*, D23S32.

(3) Ramanathan, V.; Li, F.; Ramana, M. V.; Praveen, P. S.; Kim, D.; Corrigan, C. E.; Nguyen, H.; Stone, E. A.; Schauer, J. J.; Carmichael, G. R.; et al. Atmospheric brown clouds: hemispherical and regional variations in long-range transport, absorption, and radiative forcing. *J. Geophys. Res.* **2007**, *112* (D12), D22S21.

(4) Freedman, M. A.; Hasenkopf, C. A.; Beaver, M. R.; Tolbert, M. A. Optical properties of internally mixed aerosol particles composed of dicarboxylic acids and ammonium sulfate. *J. Phys. Chem.* **2009**, *113* (48), 13584–13592.

(5) Santarpin, J. L.; Li, R.; Collins, D. R. Direct measurement of the hydration state of ambient aerosol populations. *J. Geophys. Res.* **2004**, *109*, D18209.
(6) Moore, R. H.; Raymond, T. M. HTDMA analysis of multicomponent dicarboxylic acid aerosols with comparison to UNIFAC and ZSR. *J. Geophys. Res.* **2008**, *113*, D04206.
(7) Jimenez, J. L.; Canagaratna, M. R.; Donahue, N. M.; Prevot, A. S. H.; Zhang, Q.; Kroll, J. H.; DeCarlo, P. F.; Allan, J. D.; Coe, H.; Ng, N. L. et al., Evolution of organic aerosols in the atmosphere. *Science* **2009**, *326*, 1525–1529.
(8) Wang, X.; Gao, S.; Yang, X.; Chen, H.; Chen, J.; Zhuang, G.; Surratt, J. D.; Chan, M. N.; Seinfeld, J. H. Evidence for high molecular weight nitrogen-containing organic salts in urban aerosols. *Environ. Sci. Technol.* **2010**, *44* (12), 4441–4446.
(9) Laskin, A.; Smith, J. S.; Laskin, J. Molecular characterization of nitrogen-containing organic compounds in biomass burning aerosols using high-resolution mass spectrometry. *Environ. Sci. Technol.* **2009**, *43* (10), 3764–3771.
(10) Fu, T.-M.; Jacob, D. J.; Wittrock, F.; Burrows, J. P.; Vrekoussis, M.; Henze, D. K. Global budgets of atmospheric glyoxal and methylglyoxal, and implications for formation of secondary organic aerosols. *J. Geophys. Res.* **2008**, *113*, D15303.
(11) Stavrakou, T.; Müller, J.-F.; De Smedt, I.; Van Roozendael, M.; Kanakidou, M.; Vrekoussis, M.; Wittrock, F.; Richter, A.; Burrows, J. P. The continental source of glyoxal estimated by the synergistic use of spaceborne measurements and inverse modelling. *Atmos. Chem. Phys.* **2009**, *9*, 8431–8446.
(12) Volkamer, R.; San Martini, F.; Molina, L. T.; Salcedo, D.; Jimenez, J. L.; Molina, M. J. A missing sink for gas-phase glyoxal in Mexico City: formation of secondary organic aerosol. *Geophys. Res. Lett.* **2007**, *34*, L19807.
(13) Liggio, J.; Li, S.-M.; McLaren, R. Reactive uptake of glyoxal by particulate matter. *J. Geophys. Res.* **2005**, *110*, D10304.
(14) Volkamer, R.; Ziemann, P. J.; Molina, M. J. Secondary organic aerosol formation from acetylene (C_2H_2): seed effect on SOA yields due to organic photochemistry in the aerosol aqueous phase. *Atmos. Chem. Phys.* **2009**, *9*, 1907–1928.
(15) Carlton, A. G.; Turpin, B. J.; Altieri, K. E.; Seitzinger, S.; Reff, A.; Lim, H.-J.; Ervens, B. Atmospheric oxalic acid and SOA production from glyoxal: results of aqueous photooxidation experiments. *Atmos. Environ.* **2007**, *41* (35), 7588–7602.
(16) Galloway, M. M.; Chhabra, P. S.; Chan, A. W. H.; Surratt, J. D.; Flagan, R. C.; Seinfeld, J. H.; Keutsch, F. N. Glyoxal uptake on ammonium sulphate seed aerosol: reaction products and reversibility of uptake under dark and irradiated conditions. *Atmos. Chem. Phys.* **2009**, *9*, 3331–3345.
(17) Shapiro, E. L.; Szprengiel, J.; Sareen, N.; Jen, C. N.; Giordano, M. R.; McNeill, V. F. Light-absorbing secondary organic material formed by glyoxal in aqueous aerosol mimics. *Atmos. Chem. Phys.* **2009**, *9*, 2289–2300.
(18) Noziere, B.; Dziedzic, P.; Cordova, A. Products and kinetics of the liquid-phase reaction of glyoxal catalyzed by ammonium ions (NH_4^+). *J. Phys. Chem.* **2009**, *113* (1), 231–237.
(19) De Haan, D. O.; Corrigan, A. L.; Smith, K. W.; Stroik, D. R.; Turley, J. T.; Lee, F. E.; Tolbert, M. A.; Jimenez, J. L.; Cordova, K. E.; Ferrell, G. R. Secondary organic aerosol-forming reactions of glyoxal with amino acids. *Environ. Sci. Technol.* **2009**, *43* (8), 2818–2824.
(20) De Haan, D. O.; Tolbert, M. A.; Jimenez, J. L. Atmospheric condensed-phase reactions of glyoxal with methylamine. *Geophys. Res. Lett.* **2009**, *36*, L11819.
(21) Ervens, B.; Volkamer, R. Glyoxal processing by aerosol multiphase chemistry: towards a kinetic modeling framework of secondary organic aerosol formation in aqueous particles. *Atmos. Chem. Phys.* **2010**, *10*, 8219–8244.
(22) Matsunaga, S.; Mochida, M.; Kawamura, K. Variation on the atmospheric concentrations of biogenic carbonyl compounds and their removal processes in the northern forest at Moshiri, Hokkaido Island in Japan. *J. Geophys. Res.* **2004**, *109*, D04302.
(23) Zhao, J.; Levitt, N. P.; Zhang, R.; Chen, J. Heterogeneous reactions of methylglyoxal in acidic media: implications for secondary organic aerosol formation. *Environ. Sci. Technol.* **2006**, *40* (24), 7682–7687.
(24) Kroll, J. H.; Ng, N. L.; Murphy, S. M.; Varutbangkul, V.; Flagan, R. C.; Seinfeld, J. H. Chamber studies of secondary organic aerosol growth by reactive uptake of simple carbonyl compounds. *J. Geophys. Res.* **2005**, *110*, D23207.
(25) Ervens, B.; Feingold, G.; Frost, G. J.; Kreidenweis, S. M. A modeling study of aqueous production of dicarboxylic acids: 1. Chemical pathways and speciated organic mass production. *J. Geophys. Res.* **2004**, *109*, D15205.
(26) Altieri, K. E.; Seitzinger, S. P.; Carlton, A. G.; Turpin, B. J.; Klein, G. C.; Marshall, A. G. Oligomers formed through in-cloud methylglyoxal reactions: chemical composition, properties, and mechanisms investigated by ultra-high resolution FT-ICR mass spectrometry. *Atmos. Environ.* **2008**, *42*, 1476–1490.
(27) De Haan, D. O.; Corrigan, A. L.; Tolbert, M. A.; Jimenez, J. L.; Wood, S. E.; Turley, J. J. Secondary organic aerosol formation by self-reactions of methylglyoxal and glyoxal in evaporating droplets. *Environ. Sci. Technol.* **2009**, *43* (21), 8184–8190.
(28) Sareen, N.; Schwier, A. N.; Shapiro, E. L.; Mitroo, D.; McNeill, V. F. Secondary organic material formed by methylglyoxal in aqueous aerosol mimics. *Atmos. Chem. Phys.* **2010**, *10*, 997–1016.
(29) Shumaev, K. B.; Gubkina, S. A.; Kumskova, E. M.; Shepelkova, G. S.; Ruuge, E. K.; Lankin, V. Z. Superoxide formation as a result of interaction of L-lysine with dicarbonyl compounds and its possible mechanism. *Biochem. (Moscow)* **2009**, *74* (4), 461–466.
(30) DeCarlo, P. F.; Kimmel, J. R.; Trimborn, A.; Northway, M. J.; Jayne, J. T.; Aiken, A. C.; Gonin, M.; Fuhrer, K.; Horvath, T.; Docherty, K. S. et al., Field-deployable, high-resolution, time-of-flight aerosol mass spectrometer. *Anal. Chem.* **2006**, *78* (24), 8281–8289.
(31) Canagaratna, M. R.; Jayne, J. T.; Jimenez, J. L.; Allan, J. D.; Alfarra, M. R.; Zhang, Q.; Onasch, T. B.; Drewnick, F.; Coe, H.; Middlebrook, A. et al., Chemical and microphysical characterization of ambient aerosols with the Aerodyne aerosol mass spectrometer. *Mass Spectrom. Rev.* **2007**, *26* (2), 185–222.
(32) DeCarlo, P.; Slowik, J. G.; Worsnop, D. R.; Davidovits, P.; Jimenez, J. L. Particle morphology and density characterization by combined mobility and aerodynamic diameter measurements. Part 1: Theory. *Aerosol Sci. Tecnol.* **2004**, *38*, 1185–1205.
(33) Aiken, A. C.; DeCarlo, P. F.; Jimenez, J. L. Elemental analysis of organic species with electron ionization of high-resolution mass spectrometry. *Anal. Chem.* **2007**, *79*, 8350–8358.
(34) Tolocka, M. P.; Jang, M.; Ginter, J. M.; Cox, F. J.; Kamens, R. M.; Johnston, M. V. Formation of oligomers in secondary organic aerosol. *Environ. Sci. Technol.* **2004**, *38* (5), 1428–1434.
(35) Altieri, K. E.; Carlton, A. G.; Lim, H.-J.; Turpin, B. J.; Seitzinger, S. P. Evidence for oligomer formation in clouds: reactions of isoprene oxidation products. *Environ. Sci. Technol.* **2006**, *40* (16), 4956–4960.
(36) Igawa, M.; Munger, J. W.; Hoffmann, M. R. Analysis of aldehydes in cloud- and fogwater samples by HPLC with a postcolumn reaction detector. *Environ. Sci. Technol.* **1989**, *23* (5), 556–561.
(37) Munger, J. W.; Jacob, D. J.; Daube, B. C.; Horowitz, L. W.; Keene, W. C.; Heikes, B. G. Formaldehyde, glyoxal, and methylglyoxal in air and cloudwater at a rural mountain site in central Virginia. *J. Geophys. Res.* **1995**, *100* (D5), 9325–9333.
(38) van Pinxteren, D.; Plewka, A.; Hofmann, D.; Muller, K.; Kramberger, H.; Svrcina, B.; Bachmann, K.; Jaeschke, W.; Mertes, S.; Collett, J. L., Jr.; et al. Schmucke hill cap cloud and valley stations aerosol characterisation during FEBUKO (II): organic compounds. *Atmos. Environ.* **2005**, *39*, 4305–4320.
(39) Matsumoto, K.; Kawai, S.; Igawa, M. Dominant factors controlling concentrations of aldehydes in rain, fog, dew water, and in the gas phase. *Atmos. Environ.* **2005**, *39*, 7321–7329.
(40) Mopper, K.; Zika, R. G. Free amino acids in marine rains: evidence for oxidation and potential role in nitrogen cycling. *Nature* **1987**, *325*, 246–249.
(41) Zhang, Q.; Anastasio, C. Free and combined amino compounds in atmospheric fine particles ($PM_{2.5}$) and fog waters from Northern California. *Atmos. Environ.* **2003**, *37*, 2247–2258.
(42) Krizner, H. E.; De Haan, D. O.; Kua, J. Thermodynamics and kinetics of methylglyoxal dimer formation: A computational study. *J. Phys. Chem.* **2009**, *113* (25), 6994–7001.
(43) Allan, J. D.; Jimenez, J. L.; Williams, P. I.; Alfarra, M. R.; Bower, K. N.; Jayne, J. T.; Coe, H.; Worsnop, D. R. Quantitative sampling using an Aerodyne aerosol mass spectrometer 1. Techniques of data interpretation and error analysis. *J. Geophys. Res.* **2003**, *108* (D3), 4090.
(44) Jimenez, J. L.; Bahreini, R.; Cocker, D. R. I.; Zhuang, H.; Varutbangkul, V.; Flagan, R. C.; Seinfeld, J. H.; O'Dowd, C. D.; Hoffmann, T. New particle formation from photooxidation of diiodomethane (CH_2I_2). *J. Geophys. Res.* **2003**, *108* (D10), 4318.
(45) Chan, M. N.; Choi, M. Y.; Ng, N. L.; Chan, C. K. Hygroscopicity of water-soluble organic compounds in atmospheric aerosols: amino acids and biomass derived organic species. *Environ. Sci. Technol.* **2005**, *39* (6), 1555–1562.
(46) Biskos, G.; Paulsen, D.; Russell, L. M.; Buseck, P. R.; Martin, S. T. Prompt deliquescence and efflorescence of aerosol nanoparticles. *Atmos. Chem. Phys.* **2006**, *6*, 4633–4642.

(47) Zelenyuk, A.; Imre, D.; Cuadra-Rodriguez, L. A. Evaporation of water from particles in the aerodynamic lens inlet: An experimental study. *Anal. Chem.* **2006**, *78* (19), 6942–6947.
(48) Weast, R. C. *CRC Handbook of Chemistry and Physics*; The Chemical Rubber Publishing Co.: Cleveland, OH, 1972.
(49) Denkenberger, K. A.; Moffet, R. C.; Holecek, J. C.; Rebotier, T. P.; Prather, K. A. Real-time, single-particle measurements of oligomers in aged ambient aerosol particles. *Environ. Sci. Technol.* **2007**, *41* (15), 5439–5446.
(50) Ma, Y.; Hays, M. D. Thermal extraction--two-dimensional gas chromatography--mass spectrometry with heart-cutting for nitrogen heterocyclics in biomass burning aerosols. *J. Chromatogr., Sect. A* **2008**, *1200*, 228–234.
(51) Namiki, M. Chemistry of Maillard reactions: recent studies on the browning reaction mechanism and the development of antioxidants and mutagens. *Adv. Food Res.* **1988**, *32*, 115–185.

ES102933X